

# First-Principles-Driven Model-Based Control of the Poloidal Magnetic Flux Profile at the DIII-D Tokamak<sup>\*</sup>

William Wehner<sup>\*</sup> Wenyu Shi<sup>\*</sup> Justin Barton<sup>\*</sup>  
Eugenio Schuster<sup>\*</sup> Michael L. Walker<sup>\*\*</sup> John R. Ferron<sup>\*\*</sup>  
Tim C. Luce<sup>\*\*</sup> Francesca Turco<sup>\*\*\*</sup> David A. Humphreys<sup>\*\*</sup>  
Ben G. Penaflo<sup>\*\*</sup> Robert D. Johnson<sup>\*\*</sup>

<sup>\*</sup> Lehigh University, Bethlehem, PA 18015, USA.

<sup>\*\*</sup> General Atomics, San Diego, CA 92121, USA.

<sup>\*\*\*</sup> Columbia University, New York, NY 10027, USA.

---

**Abstract:** Efficient, high-gain operation of a tokamak device requires the achievement of certain radial shapes for the toroidal current profile. The evolution in time of the toroidal current profile in tokamaks is related to the evolution of the poloidal magnetic flux profile. A model-based control approach for the regulation of the poloidal magnetic flux profile at the DIII-D tokamak is proposed in this work. The model describing the poloidal flux evolution is based on a control-oriented formulation of the magnetic diffusion equation. Auxiliary heating and current drive (H&CD) systems including electron cyclotron (EC) and neutral beam injection (NBI) along with the total plasma current are used as actuators to manipulate the profile shape. Optimal state feedback control with integral action is used to design a controller to regulate the profile around a target while rejecting disturbances. Combining the profile controller with control of the plasma stored energy is found to improve tracking performance. Simulations and experimental results are presented to demonstrate the controller's effectiveness.

---

## 1. INTRODUCTION

To initiate a fusion reaction on earth, temperatures on the order of  $10^7 - 10^9$  K are required to overcome the Coulomb repulsion between like-charged nuclei. The conventional fusion plasma, i.e. a hot gas of hydrogen ions and electrons, must be confined by magnetic fields because the high temperatures required would otherwise melt the confining structure. The motion of ionized particles are tied to the magnetic field lines by the Lorentz force. Therefore, to contain the plasma, a common solution is to close the magnetic field lines in on themselves, forming a torus as shown in Fig. 1. When the magnetic field is configured such that the field lines follow a helical path through the torus, i.e. they curve around in the poloidal direction as well as in the toroidal direction, the confinement device is called a tokamak. Following any magnetic field line a number of times around the torus a closed flux tube is mapped, a so called magnetic-flux surface, which marks points of constant poloidal magnetic flux,  $\Psi$ . A collection of such points along the plasma radial coordinate ( $\rho$  in Fig. 1) is called the poloidal magnetic flux profile.

It is anticipated that efficient, high-gain, economically viable operation of a tokamak will require the development of an advanced tokamak (AT) scenario (Romanelli and Kamendje [2009], Oyama and the JT-60 Team [2009], Strait and the DIII-D Team [2009]). The AT scenario is characterized by the optimization of various plasma

parameter profile shapes. In particular, it is necessary to optimize the safety factor profile,  $q$ , in such a way to maintain magnetohydrodynamic (MHD) stability at a high  $\beta_N$  (normalized pressure ratio) and a high fraction of the self-generated "bootstrap" current (Peters [1997]). This will enable high fusion gain and non-inductive sustainment of the plasma current for steady-state operation.

The tokamak is a high order, distributed parameter system with a large number of instabilities. Thus, an exhaustive modeling of the  $q$  profile evolution involves many nonlinear partial differential equations (PDEs). Several, reduced-complexity, control-oriented, PDE models for the current profile in tokamaks have been recently proposed. In (Ou et al. [2007]) a model valid for low confinement (L-mode) scenarios at DIII-D was developed, and in (Barton et al. [2013]) the model was extended to high confinement (H-mode) scenarios (Wesson [1984]) by incorporating the coupling between plasma magnetic and kinetic states through the bootstrap current. Similar control-oriented models have been proposed in (Witrant et al. [2007], Felici et al. [2011]).

The aim of this work is to develop a model-based feedback controller for  $q$  profile regulation during AT scenarios at DIII-D. Available actuators to manipulate the profile include the neutral beams injectors (NBI), electron cyclotron (EC) heating and current drive (H&CD), and the total plasma current. The proposed control design involves optimal state feedback with integral action to regulate the profile around a target in the presence of input disturbances. The effectiveness of the controller is examined in the final sections via simulated and experimental tests.

---

<sup>\*</sup> This work was supported by the US Department of Energy under DE-SC0001334, DE-SC0010661, and DE-FC02-04ER54698. Email contact of first author: wehner@lehigh.edu.

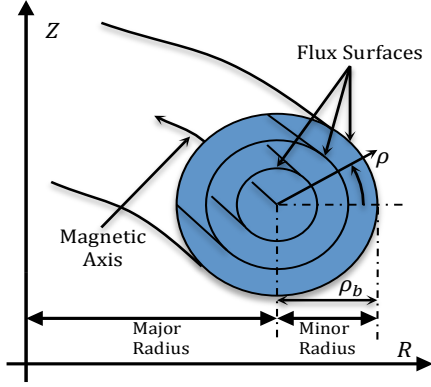


Fig. 1. Magnetic configuration of a tokamak (field lines follow a helical path around the tokamak). Flux surfaces represent points of constant poloidal magnetic flux.

## 2. MODELING THE POLOIDAL FLUX PROFILE AND INTERNAL ENERGY

In order to index the flux surfaces in Fig. 1, this work makes use of the mean effective minor radius,  $\rho$ . It can be expressed in terms of the toroidal magnetic flux,  $\Phi$ , and the toroidal field strength at the plasma center,  $B_{\phi,0}$ , i.e.  $\pi B_{\phi,0} \rho^2 = \Phi$ . Normalized  $\rho$ , denoted by  $\hat{\rho}$ , is defined as  $\rho/\rho_b$ , where  $\rho_b$  is the value of  $\rho$  at the last closed magnetic flux surface. The  $q$  profile is related to the spatial gradient of the poloidal magnetic flux,  $\Psi$ , and is defined as

$$q(\hat{\rho}, t) = \frac{d\Phi}{d\Psi} = -\frac{d\Phi}{2\pi d\psi} = -\frac{B_{\phi,0} \rho_b^2 \hat{\rho}}{\partial\psi/\partial\hat{\rho}}, \quad (1)$$

where  $t$  is the time and  $\psi$  is the poloidal stream function which is closely related to the poloidal flux, i.e.  $\Psi = 2\pi\psi$ . The plasma  $\beta_N$  is related to the volume-averaged plasma stored energy  $E$  and is defined as

$$\beta_N = \beta_t [\%] \frac{a B_{\phi,0}}{I_p [\text{MA}]}, \quad \beta_t = \frac{\langle p \rangle}{B_{\phi,0}^2 / (2\mu_0)} = \frac{(2/3)(E/V_p)}{B_{\phi,0}^2 / (2\mu_0)},$$

where  $\beta_t$  is the toroidal  $\beta$  (Wesson [1984]),  $a$  is the plasma minor radius,  $I_p$  is the total plasma current,  $p$  is the plasma kinetic pressure,  $\langle \cdot \rangle$  denotes the volume average operation  $1/V_p \int_V (\cdot) dV$ ,  $V$  is the volume enclosed by a magnetic flux surface,  $V_p$  is the total plasma volume, and  $\mu_0$  is the vacuum magnetic permeability.

In (Barton et al. [2013]), the magnetic diffusion equation (Hinton and Hazeltine [1976]) is combined with empirical correlations obtained at DIII-D for the density, temperature and non-inductive current to introduce a simplified dynamic model describing the evolution of the poloidal flux, and therefore the  $q$  profile. Here, we rewrite the model in a control-oriented form,

$$\begin{aligned} \frac{\partial\psi}{\partial t}(\hat{\rho}, t) &= \frac{f_\eta}{\hat{\rho}} \frac{\partial}{\partial\hat{\rho}} \left( \hat{\rho} D_\psi \frac{\partial\psi}{\partial\hat{\rho}} \right) u_\eta(t) + f_{\text{EC}} u_{\text{EC}}(t) \\ &+ f_{\text{CO}}^{\text{on}} u_{\text{CO}}^{\text{on}}(t) + f_{\text{CO}}^{\text{off}} u_{\text{CO}}^{\text{off}}(t) + f_{\text{BS}} \left( \frac{\partial\psi}{\partial\hat{\rho}} \right)^{-1} u_{\text{BS}}(t), \end{aligned} \quad (2)$$

with boundary conditions

$$\frac{\partial\psi}{\partial\hat{\rho}}(0, t) = 0, \quad \frac{\partial\psi}{\partial\hat{\rho}}(1, t) = -k_{I_p} I_p(t), \quad (3)$$

where  $f_\eta$ ,  $f_{\text{EC}}$ ,  $f_{\text{CO}}^{\text{on}}$ ,  $f_{\text{CO}}^{\text{off}}$ , and  $f_{\text{BS}}$  are functions of space which incorporate profile shapes for the plasma tempera-

ture, density, and plasma resistivity. The parameter  $D_\psi$  pertains to the magnetic configuration of a particular plasma equilibrium and  $k_{I_p}$  is a constant.

The input functions in (2) are nonlinear expressions of the plasma line averaged electron density,  $\bar{n}_e(t)$ , the total plasma current,  $I_p$ , the total power injected into the plasma,  $P_{\text{tot}}$ , and the auxiliary H&CD powers,  $P_{\text{EC}}$ ,  $P_{\text{CO}}^{\text{on}}$ , and  $P_{\text{CO}}^{\text{off}}$ ,

$$\begin{aligned} u_\eta(t) &= I_p(t)^{-3/2} P_{\text{tot}}(t)^{-3/4} \bar{n}_e(t)^{3/2}, \\ u_{\text{EC}}(t) &= I_p(t)^{-1/2} P_{\text{tot}}(t)^{-1/4} \bar{n}_e(t)^{-1/2} P_{\text{EC}}(t), \\ u_{\text{CO}}^{\text{on}}(t) &= I_p(t)^{-1/2} P_{\text{tot}}(t)^{-1/4} \bar{n}_e(t)^{-1/2} P_{\text{CO}}^{\text{on}}(t), \\ u_{\text{CO}}^{\text{off}}(t) &= I_p(t)^{-1/2} P_{\text{tot}}(t)^{-1/4} \bar{n}_e(t)^{-1/2} P_{\text{CO}}^{\text{off}}(t), \\ u_{\text{BS}}(t) &= I_p(t)^{-1/2} P_{\text{tot}}(t)^{-1/4} \bar{n}_e(t)^{3/2}, \end{aligned} \quad (4)$$

where  $P_{\text{EC}}$  is the total injected gyrotron power,  $P_{\text{CO}}^{\text{on}}$  is the on-axis NBI power, and  $P_{\text{CO}}^{\text{off}}$  is the off-axis NBI power. The total power injected into the plasma is the sum of auxiliary injected power, i.e.  $P_{\text{aux}} = P_{\text{EC}} + P_{\text{CO}}^{\text{on}} + P_{\text{CO}}^{\text{off}}$ , and ohmic power from the ohmic transformer coil minus the power loss by radiation,  $P_{\text{tot}} = P_{\text{ohm}} + P_{\text{aux}} - P_{\text{rad}}$ . Finally, a first order approximation of the plasma stored energy dynamics is written as

$$\frac{dE}{dt} = -\frac{E}{\tau_E} + P_{\text{tot}}(t), \quad (5)$$

where  $\tau_E$  is the global energy confinement time. The IPB98(y, 2) scaling law (ITER Physics Basis [1999]) has been adopted to model energy confinement time scaling.

### 2.1 Available actuators

The first and most effectual actuator is the total plasma current, which is regulated by the main ohmic coil (central solenoid) through a transformer effect. By controlling the total current inside the plasma, the internal  $q$  profile can be modified through resistive diffusion. Available sources of non-inductive heating and current drive are neutral beam injection (NBI) and electron cyclotron (EC) microwave injection. NBI consists of injecting beams of highly energetic neutral particles into the plasma, driving current locally and heating the plasma through collisions. The NBI system at DIII-D consists of four beam-lines, each of which has two ion sources in parallel. Each ion source can inject a maximum of 2.5 MW of power into the plasma. Currently, of the eight ion sources, four are configured to inject in the co-current direction (same direction as plasma current) aligned with the magnetic axis, referred to as co-current on-axis beams (CO-on). Two beams are configured to drive co-current with alignment  $16.5^\circ$  off-axis, referred to as co-current off-axis beams (CO-off). The last two beams are configured to inject counter-current (opposite the plasma current) with on-axis alignment, referred to as counter-current on-axis beams. Since, the counter-current beams were not expected to be available during the time of the experiment, they are not considered for control in this work. The EC system is composed of six radio-frequency (RF) wave generators (gyrotrons), which drive current and heat the plasma. The gyrotrons can inject a maximum of 0.5 MW each (3 MW in total) for a pulse length of 3 s. The final actuator is the line averaged electron density, which is controlled by gas-feed and pellet launchers.

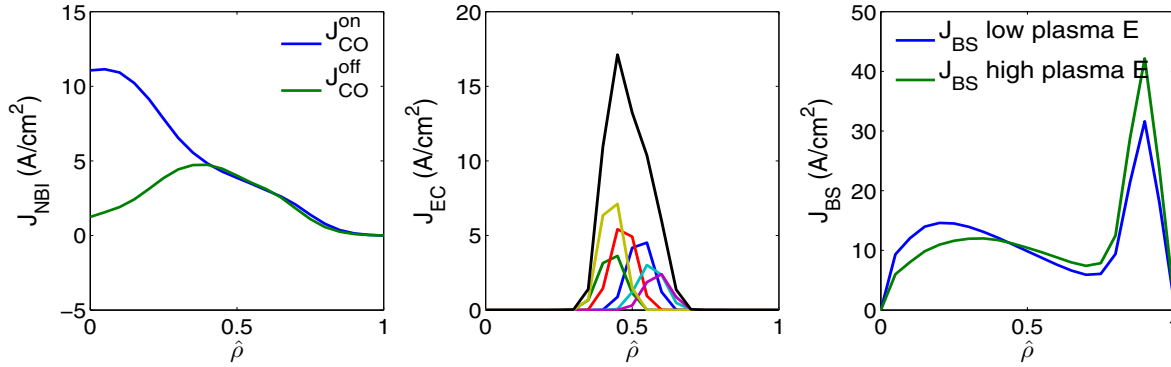


Fig. 2. Left: Current deposition profiles for the co-current on-axis (CO-on) beam group and the co-current off-axis (CO-off) beam group. Group deposition profiles are the average of the individual beam deposition profiles associated with the group. Middle: Current deposition profiles for the individual gyrotrons (colored) and the sum total EC (black). Right: Bootstrap current drive density profile at low plasma energy (blue) and high plasma energy (green). The bootstrap current increases at the plasma edge and decreases at the plasma center with increasing energy.

The driven current density profile of the neutral beam groups and gyrotrons can be seen in Fig. 2. The CO-on group drives positive current (co-current direction) mostly near the plasma center and the CO-off group drives current towards the middle of the profile (see Fig. 2 left). Notice that the CO-on group appears to be far more efficient at driving current than the CO-off group. This is because the total cross-sectional area is much smaller towards the center of plasma than around the middle. Thus while the current drive density is higher for the CO-on beams relative to the CO-off beams, the total driven current is about the same. The EC group is configured to generate a sharply localized current drive toward the mid section of the plasma (see Fig. 2 middle). An increase in plasma energy enhances the bootstrap current drive at the plasma edge and reduces it at the plasma center (see Fig. 2 right).

It can be shown that the value of  $q$  on a flux surface is inversely proportional to the plasma current enclosed by that flux surface. Hence, increasing (or decreasing) the current flow inside a flux surface reduces (or raises)  $q$  on that surface. Thus, control of the  $q$  profile is equivalent to current profile control<sup>1</sup>. Assuming the total plasma current is held constant by the ohmic coil, we can see from Fig. 2, that injecting CO-on power modifies the current distribution towards the plasma center, i.e. an increase in current flow at the center and a corresponding decrease of current flow at the edge. Similarly, injecting CO-off power modifies the current distribution away from the plasma center.

### 3. CONTROL SYSTEM STRUCTURE

In this section, a multi-input-multi-output (MIMO) feedback controller based on the first-principles-driven model (2)-(3) is proposed for the regulation of the evolution of the poloidal magnetic flux profile and thus the current profile at DIII-D. For control design, we consider the poloidal stream function relative to the boundary value, i.e.  $\bar{\psi} = \psi - \psi_b$ .

<sup>1</sup> For this reason the  $q$  profile is often simply referred to as the current profile as is the case throughout the rest of this paper.

#### 3.1 Model order reduction and linearization

To facilitate control design, the model is reduced to a finite set of ordinary differential equations (ODEs) by using finite difference approximations to the spatial derivatives. The non-dimensional domain of interest,  $\hat{\rho} = [0, 1]$ , is represented as  $l$  nodes, and the spacing between the nodes is defined as  $\Delta\hat{\rho} = 1/(l - 1)$ . Central finite difference spatial derivative approximations of  $O(\Delta\hat{\rho}^2)$  are used in the interior node region,  $2 \leq i \leq (l - 1)$  and forward and backward difference approximations of  $O(\Delta\hat{\rho}^2)$  at the boundary nodes  $i = (1, l)$ . The reduced-order discretized model is expressed as

$$\dot{X} = W(X, u), \quad (6)$$

where the model states are  $X = [\bar{\psi}_2, \bar{\psi}_3, \dots, \bar{\psi}_{l-1}]^T$ , the model inputs are  $u = [u_\eta, u_{BS}, u_{CO}^{on}, u_{CO}^{off}, u_{EC}, I_p]$ , and  $W$  is a nonlinear function. Let  $X_{FF}$  and  $u_{FF}$  represent the feedforward trajectories of the states and inputs that satisfy  $\dot{X}_{FF} = W(X_{FF}, u_{FF})$ , and let the variables  $x = X - X_{FF}$  and  $u_{FB} = u - u_{FF}$  represent perturbations around the feedforward trajectory. Inserting the perturbation variables into (6) and ignoring higher order terms results in

$$\begin{aligned} \dot{X}_{FF} + \dot{x} &= W(X_{FF}, u_{FF}) + \frac{\partial W}{\partial X}(X_{FF}, u_{FF})x \\ &+ \frac{\partial W}{\partial u}(X_{FF}, u_{FF})u_{FB}, \end{aligned}$$

from which we obtain the linear dynamics around the feedforward trajectory

$$\dot{x} = A_{FFPD}(t)x(t) + B_{FFPD}(t)u_{FB}, \quad (7)$$

where  $A_{FFPD} = \frac{\partial W}{\partial X}(X_{FF}, u_{FF})$ , and  $B_{FFPD} = \frac{\partial W}{\partial u}(X_{FF}, u_{FF})$ .

#### 3.2 Singular value decomposition

We choose to approximate the model by linearizing around a constant feedforward state and input (a stationary state<sup>2</sup>) during the flattop current phase of the discharge. Therefore, we rewrite (7) in the linear time invariant form

<sup>2</sup> A stationary state, also referred to as an ‘‘equilibrium state’’, is defined as a state where the profile gradients are in equilibrium with the particle, momentum, and heat sources and sinks. In the plasma physics community the term ‘‘steady state’’ is reserved to describe a plasma state that can be sustained without the need for an inductive current drive source.

$$\dot{x} = Ax + Bu_{FB}. \quad (8)$$

For a requested target state,  $x_t$ , let  $x_\infty$  represent the closest stationary state achievable, according to the model, which can be determined from the pseudo-inverse,  $K_{sg}^\dagger$ , of the model static gain matrix  $K_{sg} = -A^{-1}B$ . The symbol  $\dagger$  represents the Moore-Penrose pseudoinverse determined by singular value decomposition (SVD), i.e.  $K_{sg} = W\Sigma V^T$ ,  $K_{sg}^\dagger = V\Sigma^\dagger W^T$ , where  $W$  and  $V$  are unitary matrices, i.e.  $WW^T = W^T W = I$  and  $V^T V = V V^T = I$ . The pseudoinverse of the diagonal matrix  $\Sigma$  is obtained by taking the its transpose,  $\Sigma^T$ , and then taking each nonzero element with its reciprocal. The input associated with the desired target is determined from the pseudo-inverse of the static gain matrix,  $u_{FB,\infty} = K_{sg}^\dagger x_t$ , which is used to determine the closest achievable stationary state given by  $x_\infty = K_{sg} u_{FB,\infty} = K_{sg} K_{sg}^\dagger x_t$ .

We use the theory of linear quadratic optimal control to obtain a control law which regulates the system to the closest achievable stationary state while minimizing the cost function

$$J[\tilde{u}(t)] = \int_0^\infty dt \left\{ \begin{bmatrix} \tilde{x}^T(t) & \zeta^T(t) \end{bmatrix} Q \begin{bmatrix} \tilde{x}(t) \\ \zeta(t) \end{bmatrix} + \tilde{u}^T(t) R \tilde{u}(t) \right\}, \quad (9)$$

where  $\tilde{x} = x - x_\infty$ ,  $\tilde{u} = u_{FB} - u_{FB,\infty}$ ,  $Q$  positive definite,  $R$  positive semidefinite, and  $\zeta$  represents the integral states introduced for integral control. The added integral states are expressed as  $\zeta = K_\zeta \int_0^t \tilde{x}(\tau) d\tau$ , where  $K_\zeta$  is a design matrix.

Because the actuators have similar effects on the profile, the matrix  $K_{sg}$  is ill-conditioned, the ratio of the largest singular value to the smallest one is much larger than one. Therefore small deviations in the profile associated with the directions of the smaller singular values can result in unreasonably large control requests. Thus, we use a truncated singular value expansion of the static gain matrix given by,  $K_{sg,Tr} = W_{Tr}^T \Sigma_{Tr} V_{Tr}^T$ , where Tr stands for truncated and the SVD is reduced to only the  $n_{SV}$  largest singular values.

### 3.3 Choice of matrix $K_\zeta$

With the choice  $K_\zeta = W_{Tr}^T$ , we have  $(K_\zeta K_{sg,Tr} K_{sg,Tr}^\dagger) \rightarrow K_\zeta$ , since  $(W_{Tr}^T)(W_{Tr} \Sigma_{Tr} V_{Tr}^T)(V_{Tr} \Sigma_{Tr}^{-1} W_{Tr}^T) = W_{Tr}^T = K_\zeta$ , which ensures  $K_\zeta x_t \rightarrow K_\zeta x_\infty$ , since  $x_\infty \cong K_{sg,Tr} u_{FB,\infty} \cong K_{sg,Tr} K_{sg,Tr}^\dagger x_t$ . Here, we have made use of the fact that  $W_{Tr}^T W_{Tr} = I$ , and  $V_{Tr}^T V_{Tr} = I$ , but  $W_{Tr} W_{Tr}^T \neq I$ .

### 3.4 Proportional plus integral control

Written in terms of the requested target ( $\tilde{x}(t) = x(t) - K_{sg,Tr} K_{sg,Tr}^\dagger x_t(t)$ ), the control law that minimizes (9) reduces to a proportional plus integral controller of the form

$$\tilde{u}(t) = -K_p \left[ x(t) - K_{sg,Tr} K_{sg,Tr}^\dagger x_t(t) \right] - K_i K_\zeta \int_0^t d\tau \left[ x(\tau) - K_{sg,Tr} K_{sg,Tr}^\dagger x_t(\tau) \right], \quad (10)$$

where the proportional gain,  $K_p$ , and integral gain,  $K_i$ , are given by  $[K_p \ K_i] = R^{-1} \hat{B} S$ , where  $S = S^T$  is the unique

positive semi-definite solution to the algebraic Riccati equation,  $\hat{A}^T S + S \hat{A} - S \hat{B} R^{-1} \hat{B}^T S + Q = 0$ , and the system  $(\hat{A}, \hat{B})$  is constructed by augmenting the model (8) with the integrator states, i.e.

$$\begin{bmatrix} \dot{\tilde{x}} \\ \dot{\zeta} \end{bmatrix} = \underbrace{\begin{bmatrix} A & 0 \\ K_\zeta & 0 \end{bmatrix}}_{\hat{A}} \begin{bmatrix} \tilde{x} \\ \zeta \end{bmatrix} + \underbrace{\begin{bmatrix} B \\ 0 \end{bmatrix}}_{\hat{B}} \tilde{u}. \quad (11)$$

The design parameters include  $K_\zeta = W_{Tr}^T$ ,  $Q$  and  $R$ . The state weighting matrix,  $Q$ , is chosen as  $Q = \begin{bmatrix} \hat{Q} & 0 \\ 0 & \alpha_\zeta^2 I_{n_{sv}} \end{bmatrix}$ , where  $\alpha_\zeta$  is a constant that weights the integrator states relative to the model states,  $\hat{Q}$  is the weighting on the model states and  $R$  is chosen diagonal.

### 3.5 Control Signal Transformation

During experiments and simulations, the outputs of the profile controller  $u = [u_\eta, u_{BS}, u_{CO}^{on}, u_{CO}^{off}, u_{EC}, I_p]$  need to be converted to the physical actuators,  $\bar{n}_e, P_{CO}^{on}, P_{CO}^{off}, P_{EC}$ , and  $I_p$ . Inverting the nonlinear transformations (4), we can obtain expressions for the physical actuators

$$\bar{n}_e = \frac{u_{BS}}{u_\eta^{1/3}}, \quad \hat{P}_{tot} = \left( \frac{u_{BS}}{u_\eta I_p} \right)^2, \quad \hat{P}_{CO}^{on} = \frac{u_{CO}^{on} u_{BS}}{u_\eta^{2/3}}, \quad (12)$$

$$\hat{P}_{CO}^{off} = \frac{u_{CO}^{off} u_{BS}}{u_\eta^{2/3}}, \quad \text{and} \quad \hat{P}_{EC} = \frac{u_{EC} u_{BS}}{u_\eta^{2/3}}.$$

However, the inverse transformations (12) along with the constraint  $\hat{P}_{tot} = \hat{P}_{CO}^{on} + \hat{P}_{CO}^{off} + \hat{P}_{EC}$  form a set of over-constrained equations, all of which cannot be satisfied simultaneously. We desire to find the best approximation to the overdetermined system

$$X_{LS} \underbrace{\begin{bmatrix} P_{CO}^{on} & P_{CO}^{off} & P_{EC} \end{bmatrix}^T}_{P_{req}} = \underbrace{\begin{bmatrix} \hat{P}_{CO}^{on} & \hat{P}_{CO}^{off} & \hat{P}_{EC} & \hat{P}_{tot} \end{bmatrix}^T}_{\hat{P}}, \quad (13)$$

where  $P_{req}$  represents the actuator power requests to be determined,  $X_{LS}$  is the  $(4 \times 3)$  matrix  $X_{LS} = [I_3 \ \mathbf{1}]^T$ , and  $\mathbf{1}$  is a column vector of three ones. We choose a weighted least squares approach to determine the actuator power requests,

$$P_{req} = \arg \min_{P_{req}} (\hat{P} - X_{LS} P_{req})^T Q_{LS} (\hat{P} - X_{LS} P_{req}), \quad (14)$$

where  $Q_{LS}$  is a diagonal weighting matrix and the solution can be written as  $P_{req} = (Q_{LS} X_{LS})^\dagger Q_{LS} \hat{P}$ .

### 3.6 Augmenting with energy control

During simulations it was discovered that the profile tracking performance could be improved by augmenting the controller with energy control. The energy control is incorporated by adding the energy equation (5) to the linearized model (8)

$$\begin{bmatrix} \dot{x} \\ \dot{E} \end{bmatrix} = \begin{bmatrix} A & 0 \\ 0 & -1/\tau_E \end{bmatrix} \begin{bmatrix} x \\ E \end{bmatrix} + \begin{bmatrix} B & 0 \\ 0 & 1 \end{bmatrix} \begin{bmatrix} u_{FB} \\ P_{tot,kin} \end{bmatrix}, \quad (15)$$

and then proceeding with the control design as before in Section 3.2-3.5. Here we have introduced an additional control request on the total power, labeled  $P_{tot,kin}$ . Thus,

we choose the physical actuator requests as the best least squares approximation to the overdetermined system

$$X_{LS,kin} \begin{bmatrix} P_{CO}^{on} & P_{CO}^{off} & P_{EC} \end{bmatrix}^T = \begin{bmatrix} \hat{P}_{CO}^{on} & \hat{P}_{CO}^{off} & \hat{P}_{EC} & \hat{P}_{tot} & \hat{P}_{tot,kin} \end{bmatrix}^T, \quad (16)$$

where  $X_{LS,kin}$  is a matrix of the form  $X_{LS,kin} = [I_3 \ \mathbf{1} \ \mathbf{1}]^T$ .

#### 4. EXPERIMENTAL RESULTS

In this section, we present simulations and experimental results. In all the cases, the target profile is selected as the achieved profile in shot 154358. The feedforward inputs for the neutral beam groups and the plasma current are identical to the inputs of shot 154358 up to 1.5 s, at which point they are held constant. The feedforward EC power is set to 1/2 the EC power of shot 154358. Holding the plasma current and beam powers constant after 1.5 s and reducing the gyrotron power amounts to a large input disturbance.

The tuning problem consists of the selection of the diagonal elements of  $Q$  and  $R$  and the constant  $\alpha_c$  to regulate the profile as close as possible to the target. An experiment carried out at DIII-D (shot 154691) is shown in Fig. 3(a)-3(b), where we have attempted to control only the current profile without using energy control. The feedforward and requested actuator powers are plotted in Fig. 3(a), and the measured and target  $q$  profiles, together with the internal energy, are plotted in Fig. 3(b). During the experiment good profile regulation was maintained up to about 3.5 s. The profile controller attempted to correct the  $q$  profile in the plasma center after 3.5 s by saturating the CO-off NBI and EC powers while turning off the CO-on power with the goal of modifying the current distribution away from the center. Recall from Figure 2 that the CO-on NBI drives current at the plasma center while the CO-off NBI and EC drive current away from the plasma center. Thus, assuming the total plasma current remains constant, decreasing CO-on NBI power while increasing CO-off NBI and EC power should modify the current distribution away from the plasma center resulting in an increase of  $q$  at the center. However, the failure to maintain high energy in the the plasma (see Fig. 3(b)), which is not feedback controlled, may have deteriorated the off-axis bootstrap current drive effect to a level that made the  $q$  at the center remarkably more difficult to regulate in spite of the efforts by the feedback controller (see Fig. 2). It is important to point out that the the oscillations in the delivered  $I_p$  starting around 3.5 s (green line in Fig. 3(a)) are not due to the profile control algorithm, as shown by the controller requested  $I_p$  (red line in Fig. 3(a)). The cause of these oscillations remains unclear but they may have contributed to a loss in energy confinement.

Anticipating that plasma energy regulation may be critical to maintain tight control of  $q$  at the plasma center, closed-loop simulations were carried out combining current-profile and internal-energy control and are presented in Fig. 4(a)-4(b). The feedforward and requested actuator powers are plotted in Fig. 4(a), and the measured and target  $q$  profiles and internal energy are plotted in Fig. 4(b). The target profile is determined from the response of the nonlinear model (2) to the input values of shot 154358. Here, we are able to maintain good profile

tracking throughout the simulation despite large input disturbances caused by holding the feedforward inputs constant after 1.5 s. The controller increases CO-on power starting around 1.5 s to push  $q$  down towards the target at the plasma center. While the CO-on NBI group acts to regulate  $q$ , the CO-off power decreases between  $t = 2$  s and  $t = 2.5$  s to balance the internal energy at the target value of 0.8 MJ. After 2.5 s the CO-off and EC powers begin to increase to raise the internal energy up to the desired final value of approximately 1 MJ. The total plasma current is reduced slightly from its FF value to maintain tight control of  $q$  at the plasma edge. Note, in both the experiment and the simulation, the control design parameters are the same.

#### 5. SUMMARY AND CONCLUSIONS

We considered a first-principles-driven, control-oriented dynamic model describing the evolution of the poloidal flux profile and therefore the current profile during an H-mode tokamak discharge. Using finite difference, we reformulated the PDE describing the profile dynamics into a reduced order ODE model that preserves the dominant dynamics of the original parabolic PDE. Using the theory of linear-quadratic optimal control we synthesized a controller to minimize the weighted tracking error of the poloidal magnetic flux profile. First, profile control alone was considered and then performance improvements were realized by combining it with energy control. The experiment and simulation study show that the proposed controller is effective in regulating the current profile around a target in the presence of input disturbances.

#### REFERENCES

- J. Barton, W. Shi, et al. Physics-based control-oriented modeling of the safety factor profile dynamics in high performance tokamak plasmas. *Proceeding of the 52nd IEEE International Conference on Decision and Control*, 2013.
- F. Felici et al. Real-time physics-model-based simulation of the current density profile in tokamak plasmas. *Nuclear Fusion*, 51(083052), 2011.
- F. Hinton and R. Hazeltine. Theory of plasma transport in toroidal confinement systems. *Rev. Mod. Phys.*, 48: 239–308, 1976.
- ITER Physics Basis. *Nuclear Fusion*, 39:2137, 1999.
- Y. Ou et al. Towards model-based current profile control at DIII-D. *Fusion Engineering and Design*, 82:1153–1160, 2007.
- N. Oyama and the JT-60 Team. Overview of JT-60U results towards the establishment of advanced tokamak operation. *Nucl. Fusion*, 49(104007), 2009.
- A. G. Peters. The bootstrap current and its consequences. *Plasma Phys. and Control. Fusion*, 42:B47–B73, 1997.
- F. Romanelli and R. Kamendje. Overview of JET results. *Nucl. Fusion*, 49(104006), 2009.
- E. Strait and the DIII-D Team. DIII-D research in support of ITER. *Nucl. Fusion*, 49(104008), 2009.
- J. Wesson. *Tokamaks*. Oxford, UK: Clarendon Press, 1984.
- E. Witrant et al. A control-oriented model of the current profile in tokamak plasmas. *Plasma Phys. and Control. Fusion*, 49:1075–1105, 2007.

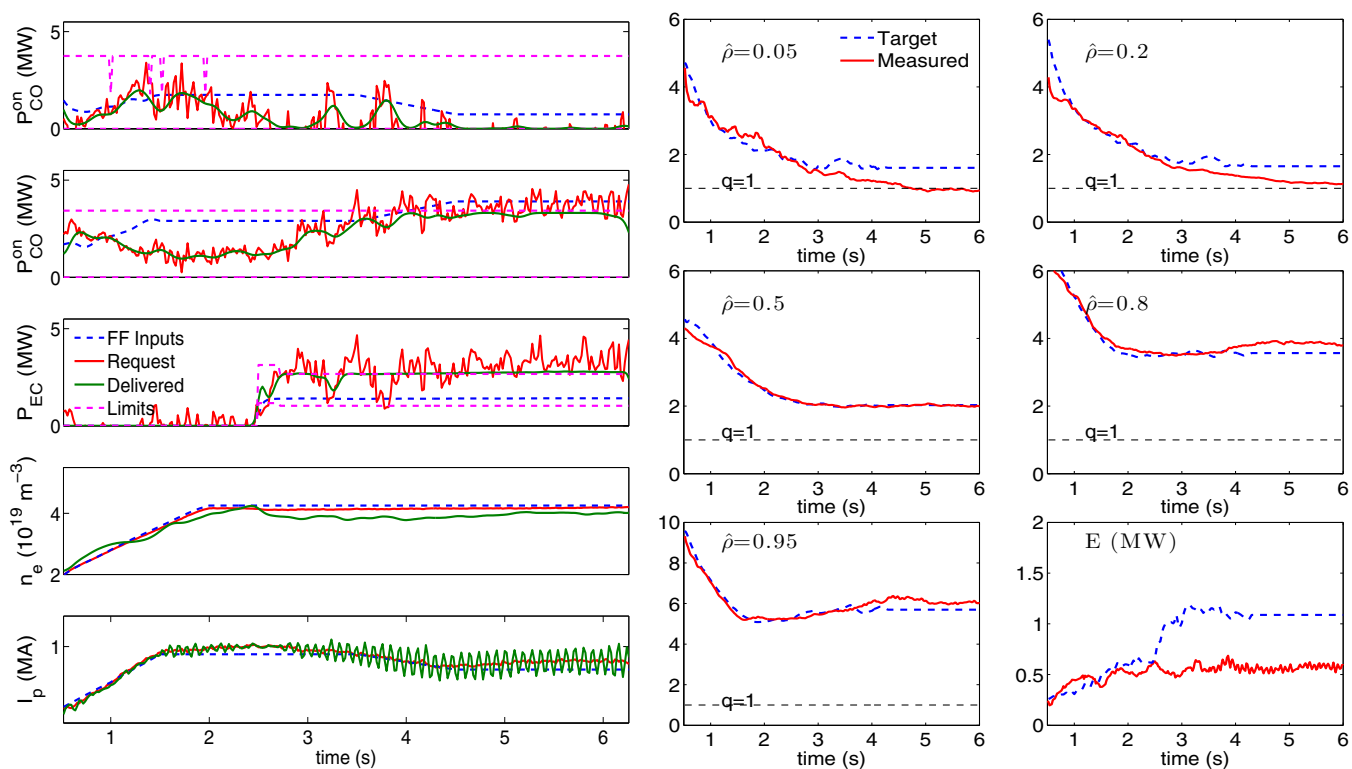


Fig. 3. DIII-D shot 154619: Current profile control experiment. Actuator values (left) and  $q$  profile and internal energy (right).

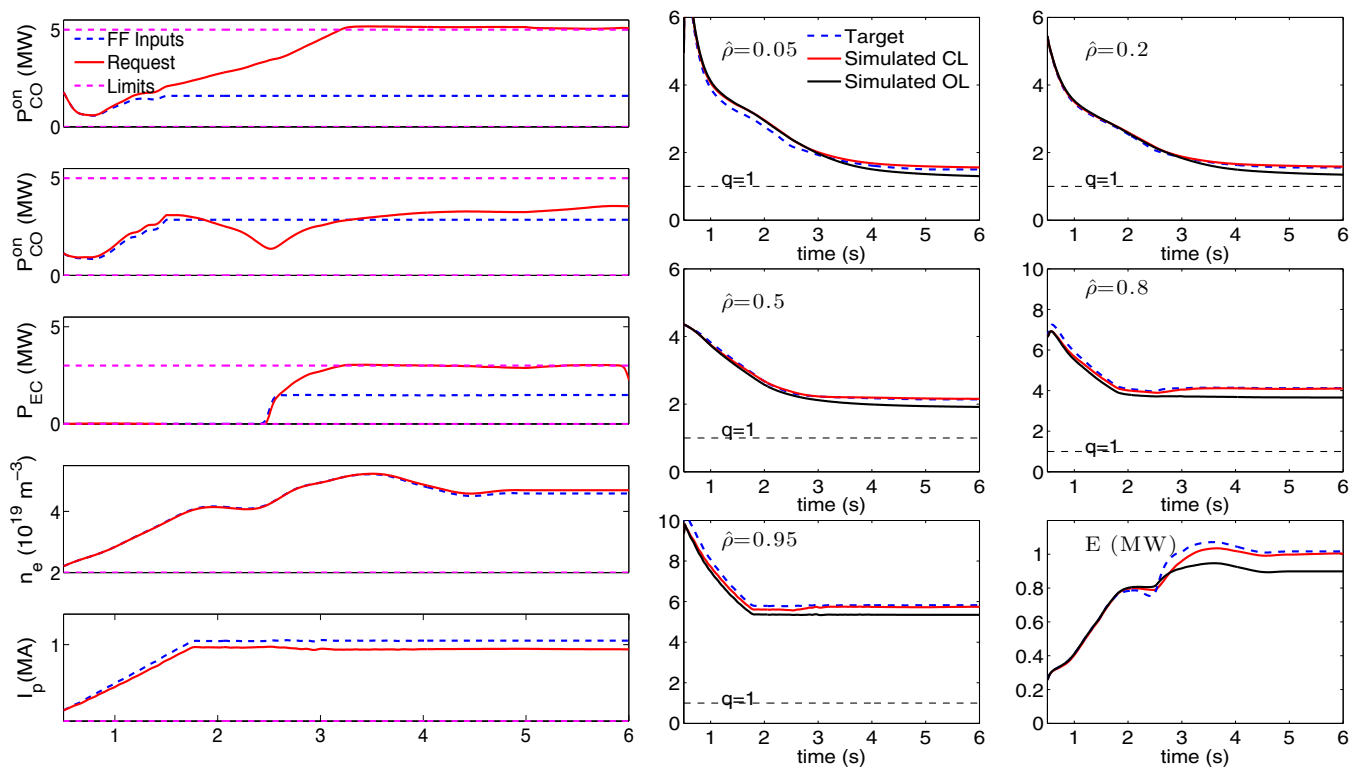


Fig. 4. Simulation: Combined current profile and energy control. Actuator values (left) and  $q$  profile and internal energy (right).